
Article:

Sarkar, A orcid.org/0000-0003-1742-2122, Kanti, F, Gulotta, A et al. (2 more authors) (2017) Aqueous Lubrication, Structure and Rheological Properties of Whey Protein Microgel Particles. Langmuir, 33 (51). pp. 14699-14708. ISSN 0743-7463

https://doi.org/10.1021/acs.langmuir.7b03627

Aqueous lubrication, structure and rheological properties of whey protein microgel particles

Anwesha Sarkar[1]*, Farah Kanti[1,2], Alessandro Gulotta[1], Brent S. Murray[1], Shuying Zhang[1]

[1]*Food Colloids and Processing Group, School of Food Science and Nutrition, University of Leeds, Leeds, LS2 9JT, United Kingdom,*

[2]*AgroSup Dijon, 26 Boulevard Docteur Petitjean, 21000 Dijon, France*

Corresponding Author

*Email: A.Sarkar@leeds.ac.uk

Food Colloids and Processing Group,

School of Food Science and Nutrition,

University of Leeds, Leeds, LS2 9JT, United Kingdom.

Abstract

Aqueous lubrication has emerged as an active research area in recent years due to its prevalence in nature in biotribological contacts and its enormous technological soft-matter applications. In this study, we designed aqueous dispersions of biocompatible whey-protein microgel particles (WPM) (10-80 vol%) cross-linked via disulfide bonding and focused on understanding their rheological, structural and biotribological properties (smooth polydimethyl siloxane (PDMS) contacts, R_a < 50 nm, ball-on-disk set up). The WPM particles (D_h = 380 nm) displayed shear-thinning behavior and good lubricating performance in the plateau boundary as well as the mixed lubrication regimes. The WPM particles facilitated lubrication between bare hydrophobic PDMS surfaces (water contact angle 108°), leading to a 10-fold reduction in boundary friction force with increased volume fraction ($\phi \geq 65\%$), largely attributed to the close packing-mediated layer of particles between the asperity contacts acting as 'true surface-separators', hydrophobic moieties of WPM binding to the non-polar surfaces and particles employing a rolling mechanism analogous to 'ball bearings', the latter supported by negligible change in size and microstructure of the WPM particles after tribology. An ultra-low boundary friction coefficient, $\mu \leq 0.03$ was achieved using WPM between O_2 plasma-treated hydrophilic PDMS contacts coated with bovine submaxillary mucin (water contact angle 47°), and electron micrographs revealed that the WPM particles spread effectively as a layer of particles even at low $\phi \sim 10\%$, forming a lubricating load-bearing film that prevented the two surfaces from true adhesive contact. However, above an optimum volume fraction, μ increased in HL+BSM surfaces due to the interpenetration of particles that possibly impeded effective rolling, explaining the slight increase in friction. These effects are reflected in the highly shear thinning nature of the WPM dispersions themselves plus the tendency for the apparent viscosity to fall as dispersions are forced to very high volume fractions. The present work

demonstrates a novel approach for providing ultra-low friction in soft polymeric surfaces using proteinaceous microgel particles that satisfy both load bearing and kinematic requirements. These findings hold great potential for designing biocompatible particles for aqueous lubrication in numerous soft matter applications.

Introduction

Microgel dispersions forms an important class of sub-micron to micron-sized, gel-like colloidal particles that essentially consist of a cross-linked network of polymer molecules.[1] The particles are swollen by the solvent (e.g., water), and have the ability to swell or de-swell depending upon the properties of the solvent, the cross-linking density of the polymer and other environmental conditions. Microgel suspensions have attracted a lot of fundamental and practical research attention owing to their unique rheological properties, which share the classical signature of both polymer solutions and 'hard' colloidal spheres.[2] These characteristics, together with their high responsiveness to environmental conditions, high surface area-to-volume ratio as compared to bulk hydrogel, and surface properties have led to a wide range of technological applications, such as surface coatings, oil recovery, foods, pharmaceutical and personal care, advanced biomaterials, lubrication and colloidal stabilizers.[3-13]

Recently, tribological characterization has also been employed to assess the application of microgels for aqueous lubrication.[14] In nature, most biological lubrication systems use an aqueous medium. Soft biological interfaces, such as the oral cavity, hip joints, respiratory tracts and eyes rely on aqueous lubricants, such as saliva or food-saliva mixture, synovial fluids, mucosal layer, or tears, respectively, to reduce sliding friction. However, water on its own is a poor lubricant and key approaches used in aqueous lubrication have involved grafting of certain amphiphilic block copolymers,[15, 16] such as polyethylene glycol (PEG) or polyethylene oxide (PEO) and adsorption of mucin[17] onto bare hydrophobic or plasma-treated hydrophilic polydimethyl siloxane (PDMS substrates). These materials have demonstrated effective aqueous lubrication, particularly under solvent conditions where the polymer was stretched out and highly solvated, creating an effective barrier layer against the bare surfaces to ensure effective boundary lubrication.

There have been efforts to understand the aqueous lubrication properties of fluid gels, i.e., concentrated dispersions of microgels made up of polysaccharides, such as, agarose,[18, 19] alginate,[20] κ-carrageenan.[21] These studies suggest that particle entrainment was a key determining factor, which reduced or increased the friction coefficient between the contacting surfaces depending upon the elasticity of the particles, their size, volume fraction, as well as the surface roughness of the tribopairs. On the other hand, surfactant-functionalized carbon microspheres of ~450 nm diameter have demonstrated their efficacy in reducing the friction between two silica surfaces via a "ball-bearing mechanism" and generating extremely low friction coefficients ($\mu \approx 0.03$) if the particles are somehow trapped and not squeezed out of the confinement.[22]

Thus, aqueous dispersions of microgels could be particularly promising, combining the lubrication behaviour of the solvent, i.e., taking advantage of the efficiency of the aqueous phase as lubricant for potential fluid film formation as "surface separator", as well as the particles, the latter providing potential "ball-bearing" effects. From a practical viewpoint, aqueous lubrication properties can be particularly important when considering interactions of microgel particles with biological environments, such as the oral cavity, where boundary- and mixed-lubrication regimes come into play and rheological measurements alone cannot completely describe the behaviour of these particles between the sliding surfaces. To our knowledge, there have been no studies on the effectiveness of sub-micron sized biopolymeric microgel particles as aqueous lubricants between soft surfaces that also evaluate the rheological behaviour of such dispersions.

In the work described here, biocompatible whey-protein microgel (WPM) particles were prepared for tribological studies via thermally induced disulphide crosslinking. The size and structure of the microgels, as well as their bulk shear rheological behaviour as a function of volume fraction were investigated. To comprehensively compare the lubricating mechanisms and

efficiency of the microgel particles at different volume fractions, two tribological contacts based on hydrophilic and hydrophobic surfaces were considered. Bare hydrophobic and O_2-plasma-treated hydrophilic PDMS/PDMS contacts at 37 °C were employed for their resemblance to wettability of external human skin surfaces (water contact angle > 100 °)[23] and internal mucosa-coated surfaces (water contact angle ≤ 70 °)[24], respectively. In the case of the O_2-plasma-treated PDMS, the substrate was coated with bovine submaxillary mucin to enhance its relevance to human oral conditions, where mucin-mediated aqueous lubrication has a crucial impact on oral health, swallowing, mouthfeel, etc. We hypothesize that the sub-micron sized WPM particles will act as aqueous "ball bearings" and the lubrication behaviour will be strongly dictated by the volume fraction of these particles entrained within the tribological contacts, thus contributing to both kinematic and load bearing properties, respectively. Although there has been one study that investigated the tribological properties of sub-micron sized poly(N-isopropylacrylamide)-graft-poly(ethylene glycol) (PNIPAAm-g-PEG) microgels,[14] to the best of our knowledge, this is the first study that reports the aqueous lubrication behaviour of biocompatible protein-based microgel particles between soft tribological contacts.

Experimental Section

Materials. Whey protein isolate powder (WPI) containing with ≥90% protein was donated by Fonterra Limited (Auckland, New Zealand). Phosphate buffer was purchased from Fisher Chemicals (Loughborough, UK). Analytical grade sodium azide was purchased from Sigma Aldrich, Gillingham, UK. Bovine submaxillary mucin BSM (Type I–S, M3895) was purchased from Sigma Aldrich, Dorset, UK. As described by the supplier, BSM contained 9-24% bound sialic acids and ≤ 2.5% free sialic acids. For the purification, BSM (30 mg/mL) was dispersed in

Milli-Q water and dialyzed in a 100 kDa molecular weight cut-off membrane followed by lyophilization, as described previously.[25] Polydimethysiloxane (PDMS, trade name Sylgard 184 elastomer kit) was obtained from Dow Corning, Midland, MI, USA. Milli-Q water (water purified to a resistivity of 18 M Ω.cm by Milli-Q apparatus, Millipore Corp., Bedford, MA, USA) was used as a solvent unless otherwise specified.

Preparation of aqueous dipersion of whey protein microgel (WPM) particles. An aqueous dispersion of whey-protein microgel (WPM) particles was prepared based on a slight modification of the methods previously described by Sarkar et al.,[4] and Murray and Phisarnchananan[13] via the disulphide bond-mediated covalent crosslinking of WPI followed by controlled shearing. Whey protein solution (10 wt%) was prepared by dissolving WPI powder in 20 mM phosphate buffer at pH 7.0 for 2 hours to ensure complete solubilization. The WPI solution was heated at 95 °C for 10 minutes and cooled at room temperature for 30 minutes followed by storage at 4 °C overnight to form a WPI gel. The gel was broken into fragments using a hand blender (HB711M, Kenwood, UK) for 10 minutes before homogenization using two passes through the Leeds Jet Homogenizer[6] operating at pressure of 300 ± 20 bar. In the Jet Homogenizer, the ratio of the gel to buffer was adjusted using two chambers of the jet homogenizer to obtain 80 vol% of WPM particles using equation (1):

$$vol\% = \frac{wt\%}{\rho} = \frac{x}{(x+y)\rho} \times 100\% \qquad (1)$$

where, ρ is the density of the gel, x is the weight of the gel, and y is the weight of the buffer at pH 7.0. To obtain aqueous dispersions with lower volume fractions of WPM (10-75 vol%), 80 vol% WPM was diluted with buffer at pH 7.0.

Rheology. A modular compact rheometer, MCR-302 (Anton Paar, Austria) was used to measure the viscosity of WPM aqueous dispersions (volume fraction, 10-80 vol%). A cone-and-plate

geometry (CP50-2, diameter: 50 mm cone angle: 2°) was used for all measurements at 25 °C. The rheometer was initialized with 0.208 mm gap between the cone and plate. The shear rate was set in the range of 0.1 s^{-1} to 50 s^{-1}, except for the extreme volume fractions (10 and 80 vol%), where the shear rate ranged from 10^{-4} to 10^{3} s^{-1} at both 25 and 37 °C. For each measurement, a small amount of sample was pipetted onto the top of the plate, excluding any air bubbles. Silicone oil was used to prevent evaporation during the measurements. Samples were left in the rheometer for approximately 5 minutes to achieve a steady state, after which the viscosity was measured. Then, after a 2 min interval, hysteresis was checked for by measurement at shear rates 50 s^{-1} to 0.1 s^{-1}. Although the normal force was nominal set to zero, during measurements it typically fluctuated between 0.3 and 0.5 N. Viscosity at each concentration was measured three times on separate samples. Viscosity values for each sample were exported from Anton Paar RheoCompass 1.13 software and analyzed using OriginPro 9.1.

Tribology. Tribological measurements of the WPM dispersions at different volume fractions (10-80 vol%) at pH 7 were performed in a Mini Traction Machine (MTM2, PCS instruments, UK) using a ball-on-disk set up to facilitate a mixed rolling and sliding contact.[26] Smooth hydrophobic polydimethylsiloxane (PDMS) balls (Ø 19 mm) and discs (Ø 46 mm) with surface roughness (R_a) < 50 nm were prepared by mixing base fluid and cross linker (10:1 w/w), as described in the specification of the Sylgard 184 kit, vacuuming to remove the entrapped air, casting using smooth stainless steel moulds and subsequently curing overnight at 70 °C.[27]

In order to investigate the effect of the surface chemistry on the lubrication properties, two types of PDMS disks were used that differed in their hydrophobicity. Bare PDMS balls and disk without any treatment were hydrophobic in nature, reported as HB hereafter. For the preparation of hydrophilic surfaces, some of the PDMS balls and disks were subjected to oxygen plasma

treatment (Zepto, Diener Electronic) at a vapor pressure of 0.4 mbar for 1 min. To avoid loss of hydrophilicity on storage, these substrates were stored immersed in Milli-Q water and used for tribology experiments within 4 days. These balls and disk are hereafter referred to as hydrophilic (HL). The HL balls and disks were coated with 100 µL of BSM solution (30 mg/mL) for 30 minutes followed by drying in N_2, as a model to represent a thin film of saliva on the substrate as observed in oral environments.[28-30] This system is hereafter reported as HL+BSM. A normal load of 2 N was used, which is equivalent to a maximum Hertzian contact pressure (P_{max}) of 100 kPa. According to Amontons' rule (1699), the coefficient of friction, µ =F/W, where F is friction force and W is the normal load was measured as a function of sliding speeds starting from high (2000 mm/s) to low (1 mm/s) as well as from low-to-high, at a sliding-to-rolling ratio (SRR) of 50% and at a fixed load (W=2 N). We only report the data obtained from high-to-low speeds, as the Stribeck curves showed negligible hysteresis. The entrainment speed of the contact between the surfaces was calculated according to the following equation (2):

$$\bar{U} = \frac{1}{2}(U' + U") \qquad (2)$$

where, $\bar{U}$ is the entrainment speed, U' is the rolling speed of the ball and U" is the sliding speed of the discs. Prior to each test, the surfaces were cleaned with acetone and rinsed with MilliQ water for the HB balls and disks. One ball-and-disk pair was used each time for an individual experiment and then discarded. The temperature used for all the tribological tests was 37 °C ± 1, aiming to mimic human oral conditions. All the experiments were carried out at pH 7 where BSM and WPM are negatively charged. The mean value of three measurements for each sample was used to plot the Stribeck curve.

Contact angle of the PDMS disks. The contact angle (θ) of MilliQ water on the PDMS disks (hydrophobic, HB; hydrophobic coated with BSM, oxygen plasma treated, HL and oxygen plasma

183 treated coated with BSM, HL+BSM) was measured using a drop-shape analysis device (OCA 25,
184 Dataphysics UK), which consisted of a computer-controlled automatic liquid deposition system
185 and a computer-based image processing system. The measuring range of the apparatus for contact
186 angle was 0-180° with a resolution of ±0.1° and each reported value is an average of more than
187 five independent measurements. Typical measurement error was less than 2°. A 500 µL volume
188 of MilliQ water was used, produced via a straight needle of 0.52 mm outer diameter and 0.26 mm
189 internal diameter, to form a sessile drop. The temperature of the chamber during the tests was at
190 20 °C to reduce evaporation of the liquid.

191 **Particle size.** The mean hydrodynamic diameter (D_h) of the WPM particles before (25 °C) and
192 after subjecting 10 vol% to tribological stress (at 37 °C) was measured via dynamic light scattering
193 (Zetasizer, Nano ZS series, Malvern Instruments, Worcestershire, UK), equipped with a 4 mW
194 He/Ne laser (wavelength = 633 nm). Sizing was performed (at 25 °C) at 10 s intervals in disposable
195 plastic cuvettes (ZEN 0040) using non-invasive backscattering at a detection angle of 173 °.
196 Measurements of the WPM particle size were based on a relative refractive index of 1.150, i.e.
197 assuming a refractive index of WPI (1.53) to 1.33 for the aqueous phase. The absorbance value of
198 the WPM particles was set at 0.001.

199 **Confocal scanning laser microscopy (CLSM).** The microstructure of 10 vol% dispersions of
200 WPM particles before and after subjecting to tribological stress (at 37 °C) was studied using a
201 Zeiss LSM 700 confocal microscope (Carl Zeiss MicroImaging GmbH, Jena, Germany). Fast
202 Green (1 mg mL^{-1} in Milli-Q water, 1:100, v/v) was used to stain WPM (He–Ne laser with an
203 excitation line at 633 nm). About 10 µL of WPM before and after the tribology experiment was
204 mixed with 10 µL of Fast Green for 15 min and imaged using a concave slide at a 63×
205 magnification.

Scanning electron microscopy (SEM). In order to directly visualize the interaction of PDMS surfaces with WPM particles, SEM observations were carried out using a FEI Quanta 200F FEG microscope (FEI Company, Eindhoven, Netherlands). A small portion of the PDMS disk (HB or HL+BSM coated) in the presence and absence of WPM particles (10 vol%), before and after being subjecting to tribological shear at 37 °C, were cut and mounted on 13 mm diameter pin stubs and coated with platinium (5 nm thick) in a Cressington 208HR sputter coater. The samples were imaged at 5 kV at 50,000 and 5,000 × magnification.

Results and Discussion

Rheology of aqueous dispersions of WPM particles. Figure 1 shows the viscosity versus shear rate for WPM dispersions at 10 and 80 vol%, with the mean and standard deviation plotted for measurements on 3 separate aliquots of the same dispersion, at 25 and 37 ºC. At both temperatures and volume fractions (ϕ), extreme shear thinning behavior was observed, with suggestions of plateau values being reached only at the low and high shear rate limits (10^{-4} and 10^{3} s^{-1}) for ϕ = 80% and 10 vol%, respectively. These shear rates represent the lowest and highest values at which reproducible data could be obtained for these samples with the rheometer used. Despite the data at ϕ = 80% apparently suggesting definite low and high shear rate limiting viscosities, it was not possible to obtain a satisfactory fit of the Cross equation:

$$\frac{\eta-\eta_\infty}{\eta_0-\eta_\infty}=\frac{1}{1+K\dot{\gamma}^m} \qquad (3)$$

:to the data across the full shear rate range; where η_∞ and η_0 are the 'infinite' and 'zero' shear rate limiting viscosities, γ the shear rate, K and m arbitrary constants. Flocculated particle networks or solutions of entangled or weakly cross-linked polymers typically follow this equation and other

workers[30] have managed to fit data of other microgels to such models, suggesting that the WPM rheology is more complex than this. However, the errors in the data at the low shear rates in particular should be noted, so that it would be unwise to interpret this much further. Of more relevance here is the fact that the viscosities at such low shear rates are unlikely to be of much relevance to conditions of the lubrication measurements (most of which will be at much higher shear rates) or the shear rates operating in the mouth, the latter being generally accepted to lie in the range of approximately 0.1 to 50 s^{-1}.[31]

It may also be noted that the viscosity curves at 25 and 37 ºC are almost indistinguishable at ϕ = 80%, whereas at ϕ = 10% the viscosities at 37 ºC are significantly higher than at 25 ºC for shear rates > 10^3 s^{-1}. The reasons for this are not clear, but possibly the WPI gel particles swell slightly at the slightly higher temperature, giving rise to slightly higher viscosities that are more noticeable at lower ϕ. Viscosity as a function of ϕ at 25 ºC was measured in more detail. Because of the difficulties in obtaining reproducible data at very high and low shear rates, plus the limited relevance of measurements in this range to lubrication, we restricted ourselves to the shear-rate range of 0.1 to 50 s^{-1} and did not attempt to find low or high shear-rate limiting viscosities at each ϕ, i.e., viscosities independent of shear rate in the low and high shear rate regions. In addition, hysteresis effects turned out to be significant – as explained below. Figure 2 compares the viscosity versus shear rate data in Figure 1 with data obtained for a completely separate preparation of WPI particle dispersions, over a wider range of ϕ, but probed over a narrower range of shear rate.

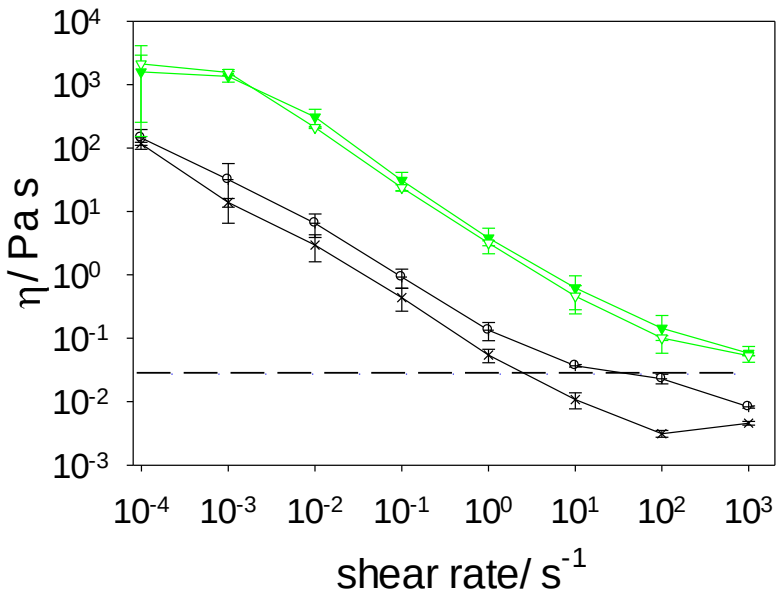

Figure 1. Viscosity (η) of WPM dispersions versus shear rate at vol% (ϕ) = 10 %, 25 ºC (grey +); 80 %, 25 ºC (green filled triangle); 10 vol%, 37 ºC (black ×); 80 vol%, 37 ºC (green open triangle). Error bars are shown for repeat sets of measurements on 3 different aliquots the same dispersion. The dashed line shows the viscosity of 70 wt.% glycerol at 25 ºC, for comparison with tribological data later.

The data for the second dispersion at ϕ = 10 vol% show very good agreement with the data described in Figure 1 for the first dispersion at the same ϕ, but the viscosities are considerably higher for the second dispersion ϕ = 80%, for example (error bars have been omitted for clarity, but they are of the same order as in Figure 2 for both sets of dispersions). In this shear-rate range, the plots of log η versus log shear rate are practically linear (and parallel), enabling fitting each set of data between ϕ = 10 to 80 vol% to a simple power law model:

$$\eta = K\left(\frac{d\gamma}{dt}\right)^{n-1} \qquad (4)$$

Equation 4 gave values of n between 0.73 between and 0.90, with all linear regression coefficients > 0.99 at each ϕ.

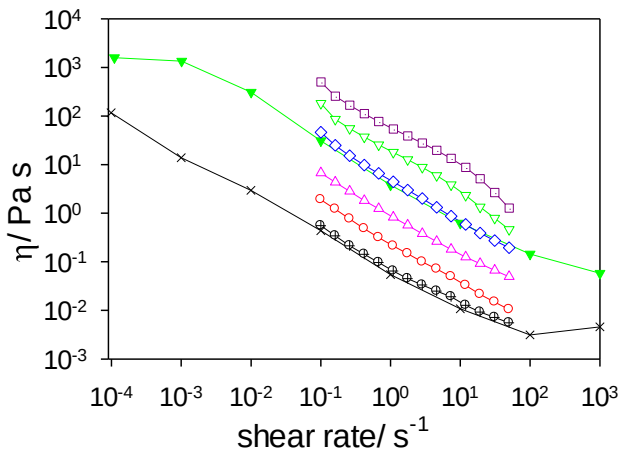

Figure 2. Comparison of viscosity (η) versus shear rate at different apparent volume fractions (ϕ) for two different preparations of WPM dispersions. Data at ϕ = 10 and 80 vol% are for the first preparation shown in Figure 1 (grey × and green filled triangle, respectively). Data for the second preparation (open symbols) are shown at ϕ = 10 % (black cross); 20 % (red circle); 50 % (pink triangle); 60% (blue diamond); 75% (purple square); 80% (green triangle).

The data of Senff & Richtering[32] for poly (N-isopropylacrylamide) (PNiPAM) microgels show a similar value of n (approximately 0.6) for the most viscous (η = 3 Pa s at 0.1 s^{-1}) system they studied, although all their systems showed lower viscosities than the WPM at equivalent effective volume fractions and shear rates, giving definite zero shear rate limiting viscosities (η_0) at much higher shear rates. This may be a reflection of a greater contribution of microgel particle aggregation to η in the case of the WPM particles. We note that in earlier work[13] on WPM rheology, a strong dependence of WPM dispersion rheology on pH was noted, attributed to

277 changes in the protein charge as a function of pH, which resulted in changes in their state of
278 aggregation. One other curious feature to note in Figure 2 for the second dispersion, is that η at ϕ
279 = 75% is apparently higher than at ϕ = 80%. Microgel particles are generally accepted as being
280 compressible to some extent and the maximum packing fractions that can be reached are generally
281 much higher than for model hard spheres.[33] Such a reversal in viscosity with ϕ is not predicted for
282 any hard-sphere models. At least part of the reason is explained in Figures 3A and 3B, which
283 show viscosities measured at 0.1 s^{-1} and 50 s^{-1}, respectively, at each ϕ where the shear rate was
284 ramped up (full lines on the Figure 3) and then ramped down (dashed lines in Figure 3), as
285 described in the Methods section. For clarity, the data points are only shown for the shear rate
286 'up' curves. It is seen that, at the 'low' (0.1 s^{-1}, Figure 3A) or 'high' (50 s^{-1}, Figure 3B) shear rates
287 the viscosity increases extremely steeply with ϕ as ϕ > 50%, as might be expected as the particles
288 become more closely packed.

289 Although the viscosities plotted in Figure 3 are not in the Newtonian regime (i.e. shear
290 thinning), the large increase in η occurs in the region of an assumed volume fraction that is typical
291 of the effective volume fraction seen in other studies – close to the random close packing limit (64
292 vol%) of truly hard spheres. However, between ϕ = 65 and 70 %, on the viscosity up curves, i.e.,
293 where the shear rate was being increased, there is a fall in apparent viscosity, followed by an
294 increase in apparent viscosity at ϕ = 75% and then another fall at ϕ = 80%. The latter explains
295 why the viscosity at 75 vol% is higher than at 80 vol% as discussed above with reference to Figure
296 2. As discussed by Senff & Richtering[32] and many others, the bulk rheology of microgel particles
297 as a function of ϕ is a complex and controversial subject, since the spheres are not hard or indeed
298 have a true surface in the usual sense, since they are particles of a gel network. Thus the surface

is expected to be porous and 'fuzzy' to some extent, whilst the particles may be deformable, as already noted, or even be able to interpenetrate to some extent.

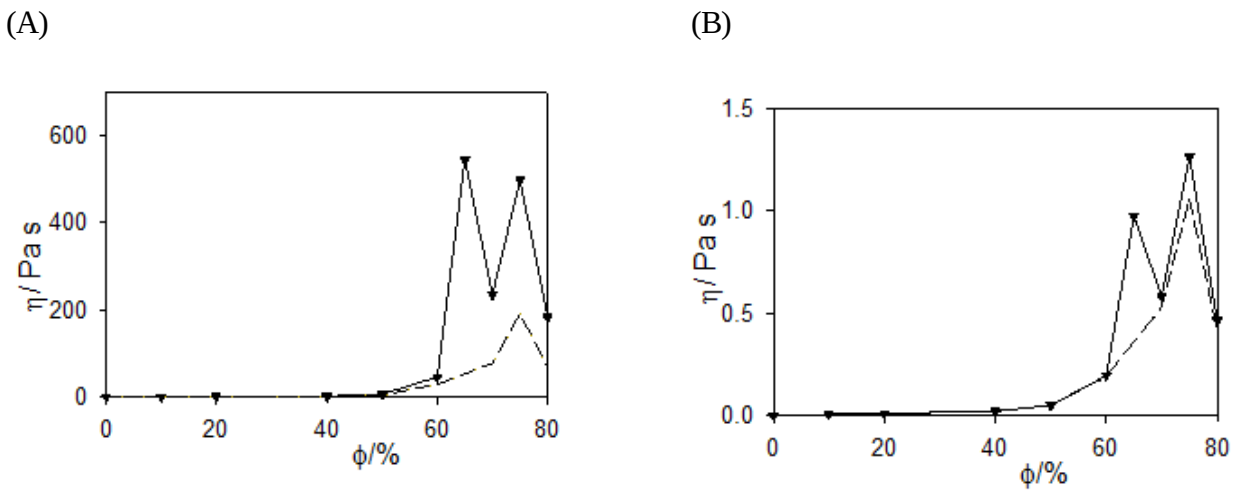

Figure 3. Detailed viscosity (η) versus apparent volume fraction (ϕ) at pH 7 (black symbols and/or lines) at shear rates of (A) 0.1 s^{-1} and (B) 50 s^{-1}, for the second dispersion referred to in Figure 2. Data are shown for the shear rate increasing from 0.1 to 50 s^{-1} (full lines) and the shear rate decreasing from 50 to 0.1 s^{-1} (dashed lines).

In our case, the calculated ϕ was based on the volume of gel broken up into particles and the volume of extra added buffer. This completely ignores the possibility of release of aqueous phase from the gel to the bulk during its disruption into microgel particles, or during the rheology measurement itself, or any swelling or shrinkage of the particles after their formation. Therefore, in line with many other studies, it is difficult to be certain of the effective volume fraction of the particles. However, it is not the purpose here to try and place the rheology of the WPM particles in the context of all detailed prior work in this area, but just to point out that the particles have similar characteristics to the behavior observed with other microgel particles.

Thus, the apparent increase and decrease in η with ϕ suggest some sort of collapse or interpenetration of the WPM particles as they are forced and sheared together at these very high volume fractions, effectively decreasing the ϕ, in other words decreasing the η and/or enhancing particle aggregation i.e. increasing the η, which might have an influence on their lubrication behavior. Upon decreasing the shear rate, (the shear down curves) all viscosities are lower than on the up curve, indicating some irreversible change (at least on the time scale of the measurements). The up and down shear rates values gradually converge at low ϕ. On the other hand, higher η is still seen at ϕ at 75 % than 80 % on the shear 'down' curve, making the collapse followed by recovery of η as a function of ϕ even more convincing. It should also be noted that we attempted to fit each η versus ϕ curve, up to the first fall in η, to the Krieger-Dougherty model of viscosity, but no value of a maximum volume packing fraction could be found for each curve that would give convergence. This is perhaps not surprising, given the hysteresis just described, which emphasizes the fact that the particles cannot be treated as hard spheres, aggregating or not.

What the detailed rheology measurements show is that the particles can give very wide ranging η values as a function of shear and shear history. In addition, high values of η persist after subjection to fairly high shear rates (50 s^{-1}) even though the systems are highly shear thinning. Thus, the particles may aggregate or interpenetrate as a function of shear and volume fraction, but they are certainly not destroyed completely by subjecting them to these conditions, so this must occur reversibly to some extent, suggesting the particles are more resilient under the conditions of shear than suggested by the moduli of the WPI gels from which they are prepared (see Supplementary Figure 1 for modulus of the whey protein gels from which WPM was prepared).

Surface properties and tribology. To gain insight into the ability of the aqueous dispersions of WPM to wet the PDMS surfaces, the water contact angle of PDMS surfaces with and without O_2-plasma treatment was determined. In general, the surface of PDMS is widely accepted as highly hydrophobic, with water contact angles reported to lie in the range of 95–110°.[30, 34] As shown in Table 1, the measured water contact angle of the HB PDMS remained fairly constant, at 108° (Table 1). Immediately after plasma treatment, the PDMS substrates became hydrophilic (30°, data not shown) due to the conversion of the methyl groups to hydroxyl and carboxyl groups at the exposed surface of PDMS, but had a rapid rate of hydrophobic recovery, as reported previously.[34, 35] In about 3 days, the contact angle reached 63° (Table 1) and remained at the same value for up to a week.

A marked decrease in contact angle ($p < 0.01$) was observed upon coating with BSM in the case of HL PDMS, i.e., the coated HL surfaces were significantly more hydrophilic than the uncoated HL surfaces (Table 1) suggesting adsorption by mucin. The contact angle was in a similar range to previously reported values of PDMS modified with mucin of porcine origin.[30] We hypothesize that such low contact angles (< 50°) might result in easier wetting of the HL disk surfaces by the WPM dispersions. The aqueous dispersions of WPM with high viscosities (Figure 2), might spread and enable the formation of a lubricating film on the substrate.

Table 1. Contact angles of water droplets measured with the sessile drop method on the different PDMS disks with or without plasma treatment and BSM coating.

PDMS Surfaces	Contact angle (θ)
HB	108.0 ± 3.0
HL	63 ± 1.0
HL+BSM	47 ± 2.0

To understand the influence of surface hydrophobicity on lubrication properties, HB (108°) and HL+BSM (47°) disks were used for tribological measurements of aqueous dispersions of WPM particles (10-80 vol%) at pH 7. Figure 4 shows the lubricating properties of the WPM particle dispersions with a range of volume fractions as a function of the entrainment speeds with HB and HL+BSM balls and disks forming the tribological contact surfaces. Based on classical tribological behavior,[36, 37] one might expect that at the boundary condition, the PDMS ball and the disk are in dry contact where both the continuous phase and/or the particles are excluded from the dry contact area. As the disk speed starts to increase, friction is expected to decrease due the dispersion material filling the gap between the surface asperities in the mixed regime. The inclusion or exclusion of WPM particles in the gaps between the contacting surfaces will largely depend on the size of the particles compared to the size of the gaps. As the speed increases further, the pressure of entrained multilayers of particles plus continuous phase should further push the two contacting surfaces apart, reducing the friction up to the beginning of hydrodynamic lubrication regime, where bulk rather than surface properties dominate.

The plateau boundary ($\bar{U} \leq 10$ mm/s) and mixed regime ($10 < \bar{U} \leq 300$ mm/s) of lubrication could be clearly identified in all the Stribeck curves (Figure 4). In case of the buffer, the elastohydrodynamic lubrication regime was also evident ($300 < \bar{U} \leq 2000$ mm/s). At $\bar{U} \geq 500$ mm/s, the friction coefficient ranged between 0.006 to 0.012, irrespective of the WPM concentration and the hydrophobicity of the substrates used. Considering the relevance to biologically relevant speeds (e.g., tongue speed), we have only focused on the boundary and mixed lubrication regimes ($\bar{U} \leq 300$ mm/s). The Stribeck curve of the phosphate buffer alone resulted in much higher friction coefficients ($\mu \geq 1.0$) in the boundary and mixed lubrication regimes. Such high interfacial friction might be due to the buffer being squeezed out from the tribo-contacts as well as the adhesive nature

of the PDMS–PDMS interface in the absence of any load-bearing lubricating film.[38] Interestingly, native whey protein solution (data not shown) gave similar friction coefficients as phosphate buffer, suggesting no formation of hydration layer between the surfaces. However, the presence of WPM particles significantly reduced the friction coefficient by up to one decade, especially in mixed lubrication regime, that is for sliding speeds 10-300 mm/s, even for extremely low volume fractions (10 vol%) (Figure 4A). The difference in lubrication properties between native whey protein/ buffer and WPM particles might be attributed to the presence of exposed hydrophobic moieties in the latter,[6] which possibly conferred adsorption and lubricity on the hydrophobic PDMS surfaces. Although WPM particles showed fairly effective lubricating properties in the mixed regime, a sharp loss in the lubricity was seen with decreasing entrainment speed (Figure 4A). This suggests that at the low volume fractions WPM particles were squeezed out from the contact region at low speeds due to low numbers of hydrophobic moieties anchored to the HB PDMS surfaces, resulting in partial direct contacts between the HB PDMS surfaces. However, such boundary friction was reduced at higher volume fractions, which is discussed in more detail below.

Focusing on the lubrication behavior of WPM particles for the bare HB PDMS surfaces (Figure 4A-F), all the aqueous dispersions of WPM particles (10-80 vol%) showed superior lubrication properties as compared to the buffer. In particular, a significant ($p < 0.05$) fall in μ values to ca. 0.06-0.4 was seen in the low-to-mid speed range ($p < 0.05$).

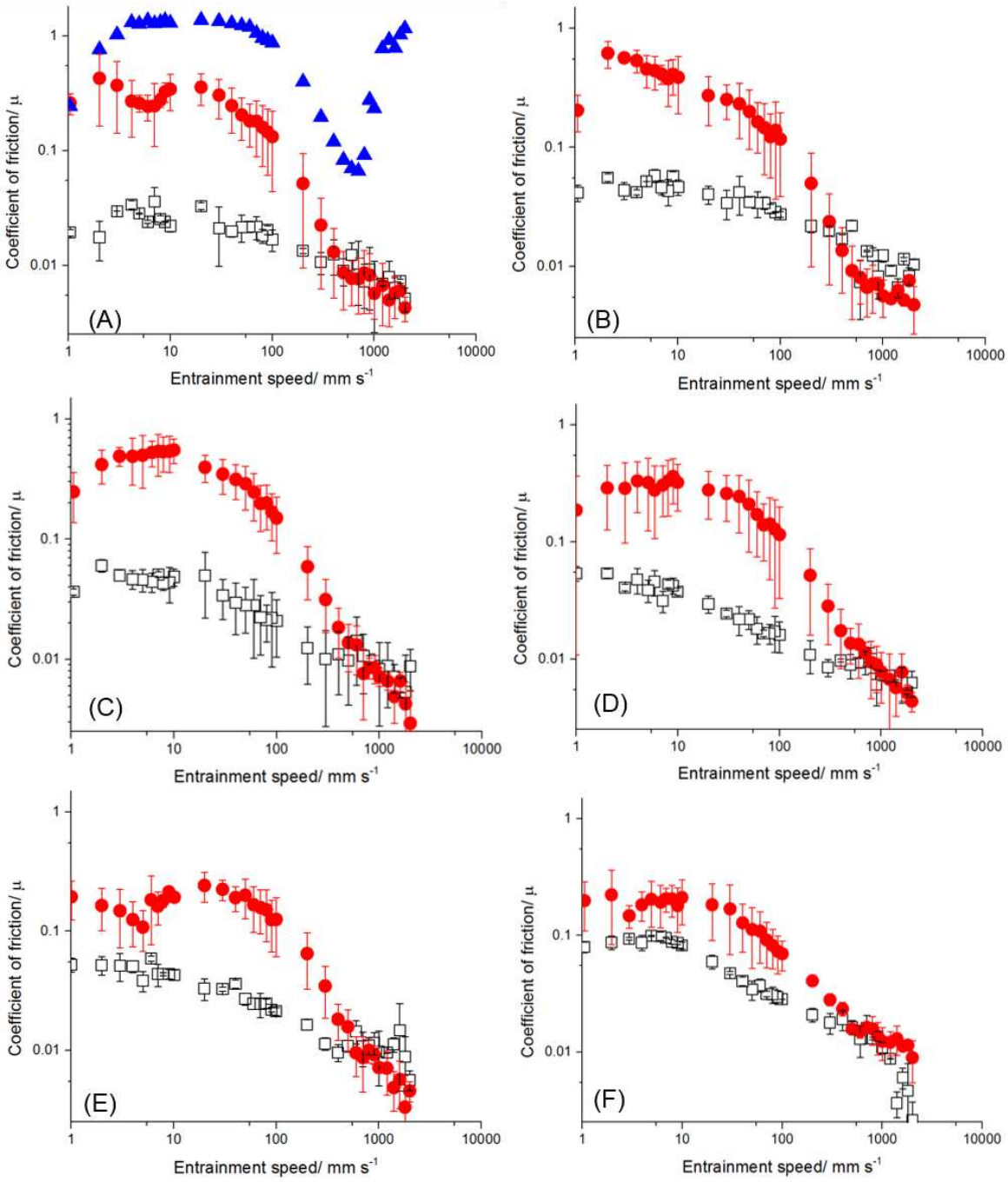

400

401 **Figure 4.** Stribeck curves of aqueous dispersions of WPM particles (10 vol%) (a), 40 vol% (b), 60
402 vol% (c), 65 vol % (d), 70 vol% (e) and 80 vol% (f) between smooth HB PDMS tribopairs (●) and
403 HL+BSM-coated PDMS tribopairs (□), showing apparent coefficient of friction measured as a
404 function of the entrainment speed. Stribeck curve of phosphate buffer is represented by ▲. Error
405 bars indicate standard deviation as obtained from three independent measurements.

The plateau boundary friction coefficient was almost 6-times lower with WPM, particularly for $\phi \geq 65$ vol% WPM (Figure 4 D-F), reaching very low μ values (ca. 0.08) compared to $\mu \approx 0.5$ at lower ϕ (10-60 vol%) (see Figures 4 A-C).

Since the PDMS surface had a R_a surface roughness of 50 nm, whilst the WPM particles had diameters 100-500 nm (discussed later), the particles could act as third body filling the gap between the asperities and result in a rolling motion, i.e., act as sub-micron scale 'ball bearings', as reported previously by St.Dennis et al.[22] and Alazemi et al.[39] with carbon microspheres of similar size range (450 ±20 nm). Having said this, carbon microspheres are expected to be much stiffer than WPM particles. Excellent lubricity with higher volume fractions of WPM (Fig. 4D-F) was also observed in the mixed regime, μ reaching values as low as 0.02 at 100 mm/s, i.e., more than 1 order of magnitude lower than that with 10-40 vol% WPM (μ = 0.4) (Fig. 4A-C). A clear trend of the dependence of friction force on ϕ (>1 N, 10 to 40 vol%; 0.69 N, 60 vol% and $\leq$ 0.3 N, 65 to 80 vol%) is seen (Figure 5A) in both boundary and mixed lubrication regimes ($p < 0.05$). Interestingly, the magnitude of the friction forces were fairly similar ($p > 0.05$) in both the mixed and boundary regimes for higher ϕ samples ($\geq$ 65 vol%).

The higher lubricity of 65-80 vol% WPM might be attributed to the higher viscosity of the dispersions and the higher number of hydrophobic moieties adsorbing to hydrophobic PDMS surfaces, inhibiting the dispersion from being squeezed out of the gap. Furthermore, the WPM particles apparently rolled easily between the HB contacts without any jamming even at high volume fractions of 80 vol%. Thus, the WPM at higher ϕ must replenish the contact region creating effective hydrated 'monolayer' of particles, filling asperity contacts (of the order of a few hundreds of nanometers). Figure 5A indicates this schematically, explaining the higher effective lubrication with PDMS-PDMS.[38] It is noteworthy that the appearance of tribological differences in the two

volume fraction regions ($\phi \geq 65\%$ and < 65 vol%) is highly congruent with the regions of most significant increase in η (Figure 2). As close packing is approached, the microgel particles might associate with each other and/or have some degree of interpenetration, helping to fill in the surface asperities more effectively, preventing surfaces from coming into contact even in the boundary condition region.

Low volume fractions of WPM showed relatively poor lubricity, with high friction forces in the mixed lubrication regime, possibly due to insufficient numbers of WPM particles replenishing the contact region (Figure 5A), as well as lower numbers of particles sticking to the surfaces. At this point it is also worth comparing the effectiveness of the WPM in reducing friction with that of a high viscosity Newtonian aqueous solution – namely 70% glycerol. Supplementary Figure 2 shows the Stribeck curve for 70% glycerol solution and the dashed line on Figure 1 shows the corresponding viscosity (η = 27 mPa s) of this solution (at 25 °C) over the same shear rate range as measured for the WPM dispersions. So at ϕ = 10 vol%, for example, the viscosity of microgel dispersion is lower than for 70% glycerol above a shear rate of ca. 1 s^{-1}, whereas the viscosity of ϕ = 80 vol% is higher than that of 70% glycerol until ca. 10^3 s^{-1}, notwithstanding the hysteresis observed in Figure 3. Once again, it is hard to compare entrainment speed with shear rate, but the fact that even the 10 vol% WPM dispersion reduces the friction even more than the 70% glycerol at the highest entrainment speed (see Supplementary Figure 2), whilst the 80 vol% gives lower friction at all entrainment speeds, points to a combined mechanism with the microgel particles, i.e., it is not just the viscosity of the dispersion that is important.

450

(A)

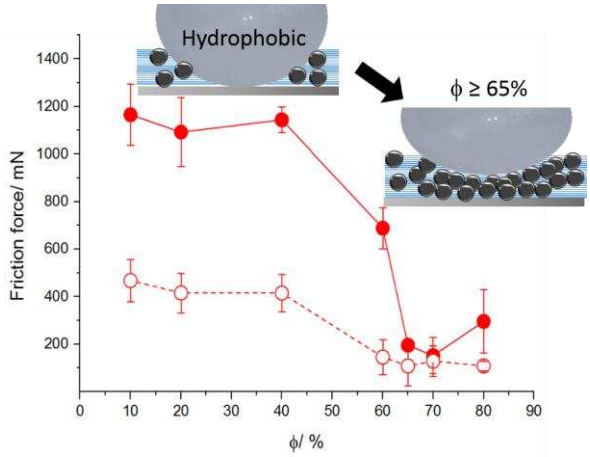

(B)

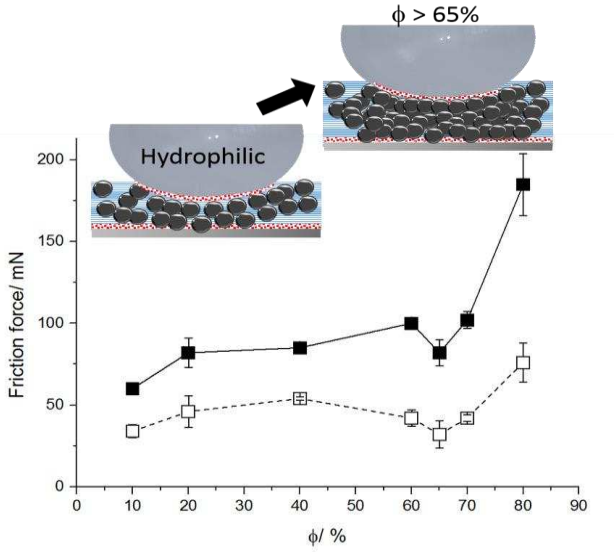

451 Figure 5. Effect of microgel volume fraction on the friction force of HB PDMS (○) (A) and
452 HL+BSM-coated PDMS (□) (B) in the boundary, U=3 mm/s (closed symbols, solid line) and
453 mixed lubrication regimes, U= 100 mm/s (open symbols, dashed line) with insets of schematic
454 representation of the proposed mechanism of microgel lubrication. Balls and disks are represented
455 in grey, microgel particles are presented by small gray spheres, the continuous phase is represented
456 by blue lines, BSM is represented by red solid dots in case of HL+BSM PDMS surfaces.

Turning to the HL+BSM surfaces in detail, the data in Figure 4 show clear differences in the Stribeck curves between the bare HB and HL+BSM surfaces, independent of the WPM volume fraction (Figure 4A-F). In the case of HL+BSM + WPM particles, the friction coefficient was reduced by more than one order of magnitude as compared to the HB surfaces at entrainment speeds (1-300 mm/s) for 10-65 vol%. At higher volume fractions (70-80 vol%), the differences in lubricity between HB and HL+BSM were not significant ($p > 0.05$) in the boundary regime. Thus, at high volume fractions WPM particles were excellent lubricants independent of hydrophobicity of the PDMS substrate.

It is noteworthy that, irrespective of WPM volume fraction, ultra-low boundary friction coefficients ($\mu \leq 0.01$) were achieved with HL+BSM. This suggests that with this surface WPM perhaps formed a monolayer preventing true adhesive contact completely and continuously flowed into the contact region with particles even at low volume fractions (10 vol%), due to effective wetting of the surfaces, as schematically illustrated in Figure 5B. Interestingly, the trend of friction force with ϕ was markedly different in case of the hydrophilic PDMS as compared to hydrophobic PDMS. It appears that there is an optimal ϕ ($\leq$ 65 vol% WPM) for effective lubrication with HL+BSM surfaces where the contact region is saturated with microgel particles. Above this volume fraction, the friction force starts to increase again, possibly due to particle close packing and aggregation/interpenetration that impedes their rolling motion rather than shear thickening due to friction between particles as seen in close packed hard sphere suspensions.

Together, these findings are in agreement with our hypothesis that the volume fraction of WPM particles play an important role in the lubricity in both HB and HL+BSM PDMS surfaces. The experiments also demonstrate for the first time that proteinaceous microgel particles can

generate ultralow friction forces ≤ 100 mN between HB PDMS and HL+BSM surfaces at higher ($\phi \geq 65$ vol%) and lower (ϕ<65 vol%) volume fractions respectively, respectively.

Size of WPM particles before and after friction measurements. The WPM particles had D_h of 380 ± 26 nm with a relatively prominent peak in the region 100-1000 nm and a small peak above 1000 nm, the latter ascribed to their aggregation (Figure 6). The 380 nm size is ~7.5 times larger than the surface mean roughness of the PDMS surfaces, i.e., it is worth re-stating that it is unlikely that the particles would get trapped between the surface asperities of the PDMS.[22] This would facilitate the ability of the particles to reduce friction by a rolling mechanism.

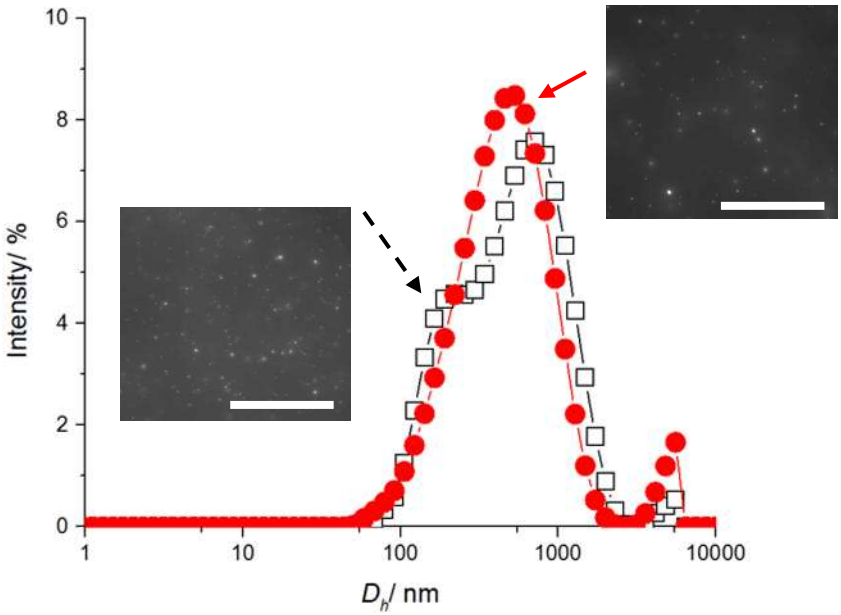

Figure 6. DLS measurements (A) of WPM particles (10 vol%) at 25.0 °C (□, dashed line), after subjecting to tribological shear at 37.0 °C (●, solid line), plotted as hydrodynamic size vs intensity, with insets representing the corresponding confocal laser microscopy images. Scale bars correspond to 50 µm, respectively.

Furthermore, there was no significant change in this D_h after subjecting the particles to tribological shear between the HB contacts surfaces, as can also can be observed in the confocal images. A slight increase in the peak in the region of 1000-10000 was observed (Figure 6), suggesting the tribological measurement induced some slight aggregation of the WPM particles, as might be expected due to the entrainment stresses. However, overall the particle size was largely preserved under the extreme boundary lubrication conditions, further supporting the suggestion of a rolling lubrication mechanism. This is also consistent with the fact that the pressure applied (2 N normal load) was almost 2-3 orders of magnitude lower than the yield stress of the WPM gels from which particles were formed (Supplementary Figure 1).

Morphology of WPM particles and surfaces before and after friction measurements. Figures 7 and 8 show the SEM images of the HB, and HL+BSM surfaces used, before and after tribology measurements. The HB disks had the smoothest surfaces (Figure 7), whereas some scratches and channels were visible in HL+ BSM surface (Figure 8). The imperfections in the latter are probably due to the plasma treatment, as reported previously.[40] The HB PDMS disks with WPM particles showed a rather sparse distribution of particles on the surface, suggesting that there was limited retention of the hydrophilic particles on the hydrophobic substrate (Figure 4), which might be expected, especially with 10 vol% particles. After the tribological measurements, there were some visible remnants of particles, which might indicate some particle abrasion while still maintaining some degree of lubricity, as observed in Figure 4a. In contrast, Figure 8 shows that the HL+BSM surfaces were almost completely covered by a jammed layer of WPM particles, indicating better binding of the WPM particles to the hydrophilic substrates, congruent with the findings of reduced μ (see Figure 4) irrespective of the volume fraction. Figure 8 shows that, after application of the tribological stresses, a significant proportion of particles remained intact and appeared to wet the

surfaces more evenly. Compared to the HB surfaces, this seems to fit in with the much lower friction forces as observed with the HL surfaces (see Figure 4a) and the suggested rolling mechanism of WPM particles.

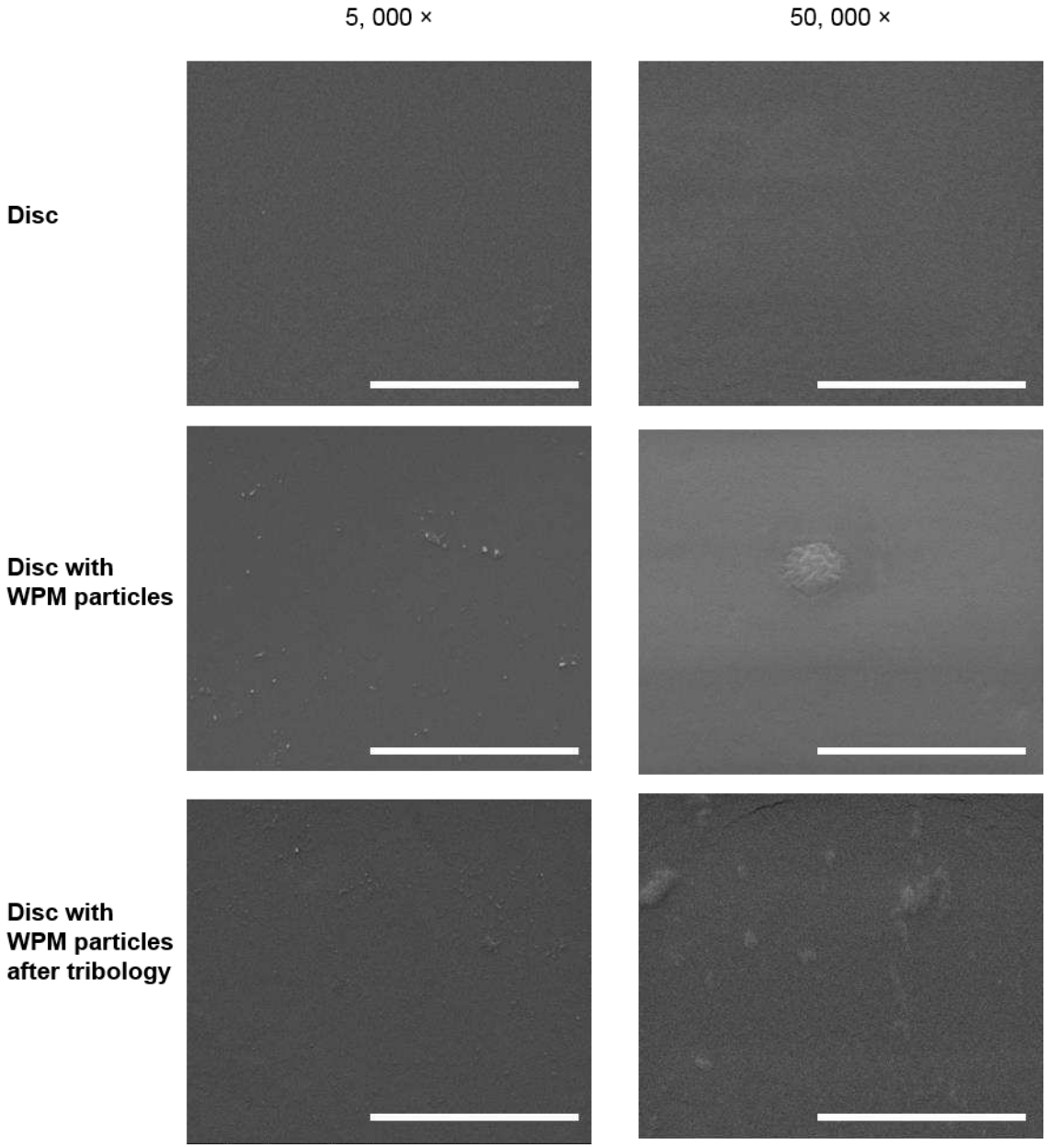

Figure 7. SEM images of HB PDMS disks in absence or presence WPM particles (10 vol%) before and after subjecting to tribological shear. Scale bars in 5,000 × and 50,000 × correspond to 30 and 3 μm, respectively.

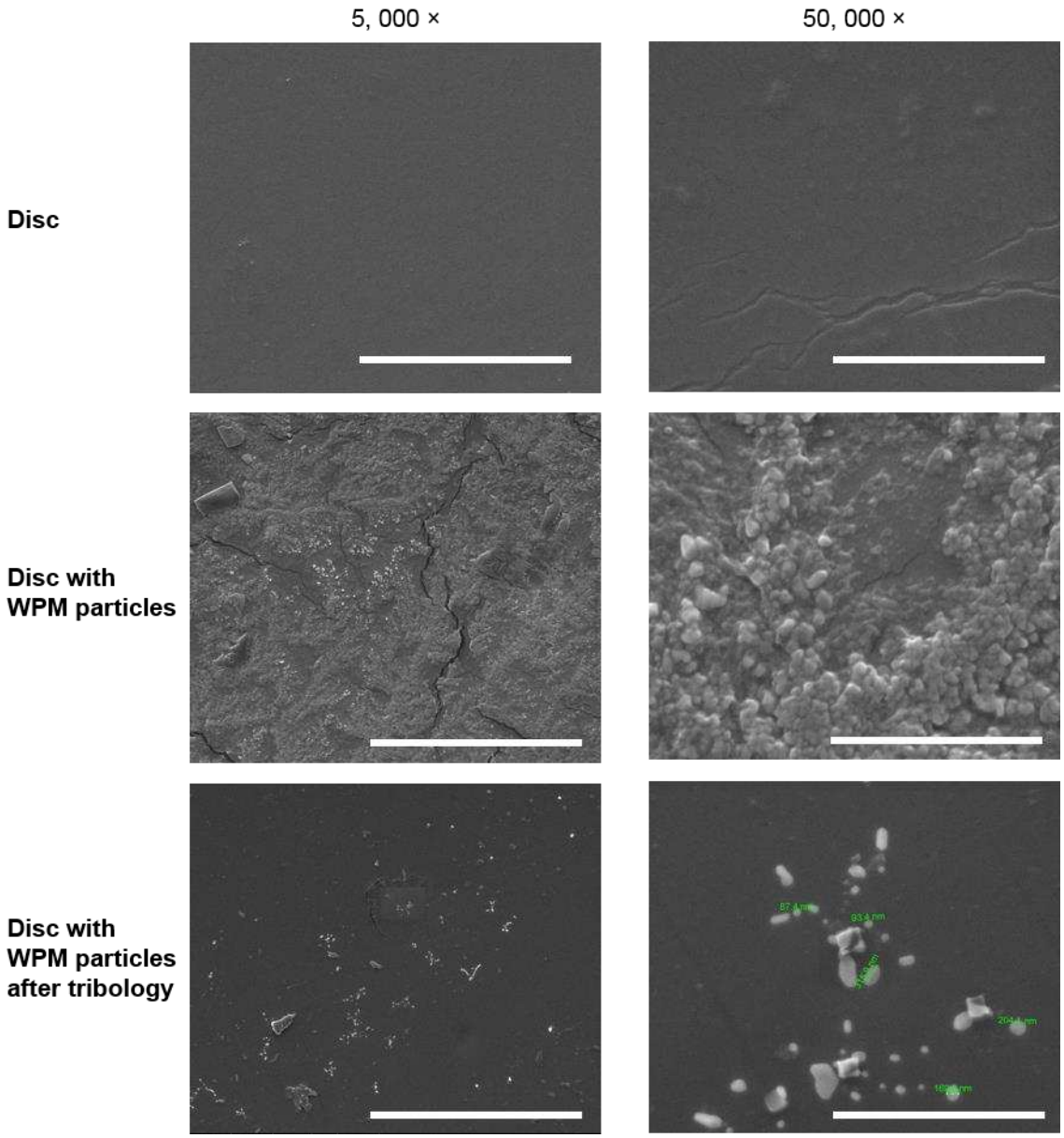

524

525

526 **Figure 8.** SEM images of HL+BSM PDMS disks in absence or presence WPM particles (10 vol%)

527 before and after subjecting to tribological shear. Scale bars in 5,000 × and 50,000 × correspond to

528 30 and 3 μm, respectively.

529

Interestingly, the particles also did not show any apparent change in particle morphology on exposure to tribological shear when examined at higher magnification (Figure 8) and consistent with the only slight change observed in the DLS data. The latter (see Figure 6) showed a change in the size distribution of particles on the surface, but no significant change in mean D_h. The WPM particles in the SEM images before and after shear appeared to be rather smaller compared with the DLS data, but this is probably due to the inevitable shrinking during sample preparation for SEM. The HL+BSM surfaces with WPM showed the presence of some degree of inter-connected WPM particles. This might be due to depletion flocculation of the weakly negatively charged WPM with the BSM at pH 7 [29] or the shearing processes in the narrow gap between the surfaces. The SEM micrographs of the WPM particles on the PDMS surfaces before and after tribology are also consistent with the rheology results, which inferred possible interpenetration of particles as a function of shear whilst they did not irreversibly collapse.

It is also worth noting that some WPM particles showed some sharp facets (almost like crystals), which might be expected to impede rolling, although, such particles would favour a 'flip-flop' mechanism of particle faces between surfaces. These flat sided objects appear more prevalent after shearing, but there are far more particles visible on the surfaces before shearing, and the densely packed layer makes it difficult to determine the fraction of more flat sided particles over more rounded ones. It is possible that some separation of the two types of particles occurs during shearing and that the flat-sided type sticks better to the surfaces and so are apparently more prevalent than the round ones in the SEM images. However, it is difficult to compare with certainty the sphericity of the WPM particles embedded on the PDMS surfaces before and after tribology because of the possible effects of preparation for SEM on particle morphology, as already mentioned. Also, it is important to understand the change (if any) of the sphericity of the particles

553 after rheological measurements. Hence, additional high-resolution characterization, before and
554 after rheology as well as shearing in confinement between the surfaces, is needed in order to clarify
555 if one type of WPM particle morphology is more important than another in providing the ultra-
556 low friction observed.
557

558 **Conclusions**

559 The aqueous dispersions of WPM particles have been shown to be efficient boundary lubricants
560 in PDMS-PDMS contacts. The coefficient of friction μ varied as a function of volume fraction of
561 WPM used, closely associated with the packing fraction when confined between the HB PDMS (ϕ
562 $\geq$ 65%) or HL+BSM (ϕ < 65%) contact surfaces. The key mechanism proposed to prevent adhesion
563 and lower friction between the sliding contacts was probably a rolling mechanism, analogous to
564 that provided by ball-bearings as well as load bearing ability attributed to the viscosity of closely
565 packed WPM particles. The motion of the top surface causes the WPM particles to roll, while the
566 confined region was continuously replenished from the surrounding medium with WPM particles
567 at higher volume fraction. In addition, the hydrophobic moieties of the WPM particles ensured
568 effective adsorption to the hydrophobic PDMS surfaces while the hydrophilic moieties of WPM
569 formed a true hydration layer, in other words a 'surface-separator'. In the case of the hydrophilic
570 PDMS surfaces, the effective wetting by WPM allowed reduction of boundary friction even at low
571 volume fractions (ϕ =10-40 vol%), supported by electron microscopy observations. However,
572 above an optimum volume fraction, the interpenetration of particles possibly impeded effective
573 rolling, explaining the slight increase in friction. These findings provide a fundamental
574 understanding of the rheological and aqueous lubrication properties of proteinaceous microgel
575 particles and may lead to innovative strategies for the development of food, drugs, personal care,

biological and biomaterial applications, exploiting their excellent aqueous lubrication and shear thinning properties.

Author information

Corresponding Author

*Email: A.Sarkar@leeds.ac.uk

Food Colloids and Processing Group,

School of Food Science and Nutrition,

University of Leeds, Leeds, LS2 9JT, United Kingdom.

Notes

The authors declare no competing financial interests

Acknowledgements

The European Research Council is acknowledged for its financial support (Funding scheme, ERC Starting Grant 2017, Project number 757993) for this work. Author (AS) is grateful to Prof. Nicholas Spencer (Dept. of Material Science, ETH Zurich, Switzerland) for the useful discussion and would like to thank Dr. Simon Connell for allowing us to use the plasma chamber in School of Physics and Astronomy at University of Leeds, UK. Authors would like to gratefully acknowledge the contributions of Martin Fuller for his technical support in electron microscopy imaging at Bio-imaging Facility within the Faculty of Biological Sciences of the University of Leeds.

References

1. Dickinson, E., Microgels — An alternative colloidal ingredient for stabilization of food emulsions. Trends in Food Science & Technology **2015,** 43, (2), 178-188.

2. Shewan, H. M.; Stokes, J. R., Review of techniques to manufacture micro-hydrogel particles for the food industry and their applications. Journal of Food Engineering **2013,** 119, (4), 781-792.

3. Mewis, J.; Wagner, N. J., Current trends in suspension rheology. Journal of Non-Newtonian Fluid Mechanics **2009,** 157, (3), 147-150.

4. Sarkar, A.; Murray, B.; Holmes, M.; Ettelaie, R.; Abdalla, A.; Yang, X., In vitro digestion of Pickering emulsions stabilized by soft whey protein microgel particles: influence of thermal treatment. Soft Matter **2016,** 12, (15), 3558-3569.

5. Torres, O.; Murray, B.; Sarkar, A., Emulsion microgel particles: Novel encapsulation strategy for lipophilic molecules. Trends in Food Science & Technology **2016,** 55, (9), 98-108.

6. Torres, O.; Murray, B.; Sarkar, A., Design of novel emulsion microgel particles of tuneable size. Food Hydrocolloids **2017,** 71, (10), 47-59.

7. Bradley, M.; Vincent, B.; Warren, N.; Eastoe, J.; Vesperinas, A., Photoresponsive surfactants in microgel dispersions. Langmuir **2006,** 22, (1), 101-105.

8. Son, H. A.; Choi, S. K.; Jeong, E. S.; Kim, B.; Kim, H. T.; Sung, W. M.; Kim, J. W., Microbial activation of bacillus subtilis-immobilized microgel particles for enhanced oil recovery. Langmuir **2016,** 32, (35), 8909-8915.

9. Saunders, B. R.; Vincent, B., Microgel particles as model colloids: theory, properties and applications. Advances in Colloid and Interface Science **1999,** 80, (1), 1-25.

10. Liu, G.; Liu, Z.; Li, N.; Wang, X.; Zhou, F.; Liu, W., Hairy polyelectrolyte brushes-grafted thermosensitive microgels as artificial synovial fluid for simultaneous biomimetic lubrication and arthritis treatment. ACS Applied Materials & Interfaces **2014,** 6, (22), 20452-20463.

11. Torres, O.; Tena, N. M.; Murray, B.; Sarkar, A., Novel starch based emulsion gels and emulsion microgel particles: Design, structure and rheology. Carbohydrate Polymers **2017,** 178, (Supplement C), 86-94.

12. Nicolai, T.; Murray, B., Particle stabilized water in water emulsions. Food Hydrocolloids **2017,** 68, (Supplement C), 157-163.

13. Murray, B. S.; Phisarnchananan, N., Whey protein microgel particles as stabilizers of waxy corn starch + locust bean gum water-in-water emulsions. Food Hydrocolloids **2016,** 56, (Supplement C), 161-169.

14. Liu, G.; Wang, X.; Zhou, F.; Liu, W., Tuning the tribological property with thermal sensitive microgels for aqueous lubrication. ACS Applied Materials & Interfaces **2013,** 5, (21), 10842-10852.

15. Lee, S.; Iten, R.; Müller, M.; Spencer, N. D., Influence of molecular architecture on the *adsorption of Poly(ethylene oxide)−Poly(propylene oxide)−Poly(ethylene oxide) on PDMS* surfaces and implications for aqueous lubrication. Macromolecules **2004,** 37, (22), 8349-8356.

16. Lee, S.; Müller, M.; Ratoi-Salagean, M.; Vörös, J.; Pasche, S.; De Paul, S. M.; Spikes, H. A.; Textor, M.; Spencer, N. D., Boundary lubrication of oxide surfaces by Poly(L-lysine)-g-poly(ethylene glycol) (PLL-g-PEG) in AQUEOUS MEDIA. Tribology Letters **2003,** 15, (3), 231-239.

17. Lee, S.; Müller, M.; Rezwan, K.; Spencer, N. D., Porcine gastric mucin (pgm) at the *water/poly(dimethylsiloxane) (PDMS) interface: Influence of pH and ionic strength on its* conformation, adsorption, and aqueous lubrication properties. Langmuir **2005,** 21, (18), 8344-8353.

18. Gabriele, A.; Spyropoulos, F.; Norton, I. T., A conceptual model for fluid gel lubrication. Soft Matter **2010,** 6, (17), 4205-4213.

19. Fernández Farrés, I.; Norton, I. T., The influence of co-solutes on tribology of agar fluid gels. Food Hydrocolloids **2015,** 45, 186-195.

20. Fernández Farrés, I.; Douaire, M.; Norton, I. T., Rheology and tribological properties of Ca-alginate fluid gels produced by diffusion-controlled method. Food Hydrocolloids **2013,** 32, (1), 115-122.

21. Garrec, D. A.; Norton, I. T., Kappa carrageenan fluid gel material properties. Part 2: Tribology. Food Hydrocolloids **2013,** 33, (1), 160-167.

22. St.Dennis, J. E.; Jin, K.; John, V. T.; Pesika, N. S., Carbon microspheres as ball bearings in aqueous-based lubrication. ACS Applied Materials & Interfaces **2011,** 3, (7), 2215-2218.

23. Ginn, M. E.; Noyes, C. M.; Jungermann, E., The contact angle of water on viable human skin. Journal of Colloid and Interface Science **1968,** 26, (2), 146-151.

24. Busscher, H. J., Wettability of surfaces in the oral cavity. In Modern approaches to wettability: Theory and applications, Schrader, M. E.; Loeb, G. I., Eds. Springer US: Boston, MA, 1992; pp 249-261.

25. Ahn, J.; Crouzier, T.; Ribbeck, K.; Rubner, M. F.; Cohen, R. E., Tuning the properties of mucin via layer-by-layer assembly. Biomacromolecules **2015,** 16, (1), 228-235.

26. Laguna, L.; Farrell, G.; Bryant, M.; Morina, A.; Sarkar, A., Relating rheology and tribology of commercial dairy colloids to sensory perception. Food & Function **2016,** 8, (2), 563-573.

27. Scaraggi, M.; Carbone, G.; Dini, D., Experimental evidence of micro-EHL lubrication in rough soft contacts. Tribology Letters **2011,** 43, (2), 169-174.

28. Bongaerts, J. H. H.; Rossetti, D.; Stokes, J. R., The lubricating properties of human whole saliva. Tribology Letters **2007,** 27, (3), 277-287.

29. Sarkar, A.; Goh, K. K. T.; Singh, H., Colloidal stability and interactions of milk-protein-stabilized emulsions in an artificial saliva. Food Hydrocolloids **2009,** 23, (5), 1270-1278.

30. Yakubov, G. E.; McColl, J.; Bongaerts, J. H. H.; Ramsden, J. J., Viscous boundary lubrication of hydrophobic surfaces by mucin. Langmuir **2009,** 25, (4), 2313-2321.

31. Sherman, P.; Deghaidy, F. S., Force-deformation conditions associated with the evaluation of brittleness and crispness in selected foods. Journal of Texture Studies **1978,** 9, (4), 437-459.

32. Senff, H.; Richtering, W., Influence of cross-link density on rheological properties of temperature-sensitive microgel suspensions. Colloid and Polymer Science **2000,** 278, (9), 830-840.

33. Stokes, J. R., Rheology of industrially relevant microgels. In Microgel Suspensions, Fernandez-Nieves, A.; Wyss, H. M.; Mattsson, J.; Weitz, D. A., Eds. Wiley-VCH Verlag GmbH & Co. KGaA: 2011; pp 327-353.

34. Lawton, R. A.; Price, C. R.; Runge, A. F.; Doherty, W. J.; Saavedra, S. S., Air plasma treatment of submicron thick PDMS polymer films: effect of oxidation time and storage conditions. Colloids and Surfaces A: Physicochemical and Engineering Aspects **2005,** 253, (1), 213-215.

35. Murthy, R.; Cox, C. D.; Hahn, M. S.; Grunlan, M. A., Protein-*resistant silicones:* Incorporation of poly(ethylene oxide) via siloxane tethers. Biomacromolecules **2007,** 8, (10), 3244-3252.

36. Stokes, J. R.; Boehm, M. W.; Baier, S. K., Oral processing, texture and mouthfeel: From rheology to tribology and beyond. Current Opinion in Colloid & Interface Science **2013,** 18, (4), 349-359.

37. Laguna, L.; Sarkar, A., Oral tribology: update on the relevance to study astringency in wines. Tribology - Materials, Surfaces & Interfaces **2017,** 11, (2), 116-123.

38. Madsen, J. B.; Sotres, J.; Pakkanen, K. I.; Efler, P.; Svensson, B.; Abou Hachem, M.; Arnebrant, T.; Lee, S., Structural and mechanical properties of thin films of bovine submaxillary mucin versus porcine gastric mucin on a hydrophobic surface in aqueous solutions. Langmuir **2016,** 32, (38), 9687-9696.

39. Alazemi, A. A.; Etacheri, V.; Dysart, A. D.; Stacke, L.-E.; Pol, V. G.; Sadeghi, F., Ultrasmooth submicrometer carbon spheres as lubricant additives for friction and wear reduction. ACS Applied Materials & Interfaces **2015,** 7, (9), 5514-5521.

40. Bodas, D.; Khan-Malek, C., Hydrophilization and hydrophobic recovery of PDMS by oxygen plasma and chemical treatment—An SEM investigation. Sensors and Actuators B: Chemical **2007,** 123, (1), 368-373.